

Band-gap renormalization in semiconductors with multiple inequivalent valleys

H. Kalt* and M. Rinker

Max-Planck-Institut für Festkörperforschung, Heisenbergstrasse 1, D-7000 Stuttgart 80, Federal Republic of Germany

(Received 12 July 1991)

The narrowing of direct and indirect band gaps is investigated in highly excited semiconductor materials with multiple inequivalent valleys in the conduction band. The model substance chosen is $\text{Al}_x\text{Ga}_{1-x}\text{As}$ close to the crossover from a direct-band-gap to an indirect-band-gap semiconductor. A theoretical model is presented, which is an extension of the universal formula for band-gap renormalization (BGR) to a multivalley scenario. This model accounts explicitly for the electron-exchange contribution to BGR in each conduction-band minimum. Its applicability to the case of high carrier densities is demonstrated by comparison to band-gap energies experimentally determined from time-resolved luminescence spectra. In a scenario of essentially unoccupied higher-energy conduction-band minima, one finds a renormalization of the fundamental gap by full correlation and exchange effects. The higher-energy gaps, on the other hand, narrow mainly due to the interactions between the holes in the valence band, while the electron-exchange effect in the empty valleys is negligible. The case of the electrons being distributed among several minima, such as in direct band-gap $\text{Al}_x\text{Ga}_{1-x}\text{As}$ just below the crossover point, is treated with a self-consistent routine for the population and renormalization of each valley. The agreement with experimental data is excellent and the alleged enhancement of the BGR in this scenario is quantitatively explained. The differential renormalization of minima with different populations is utilized to achieve a laser-induced transition from a direct-band-gap to an indirect-band-gap semiconductor in $\text{Al}_{0.42}\text{Ga}_{0.58}\text{As}$. Crossings of various conduction-band minima due to BGR is predicted from the self-consistent multivalley model and demonstrated by the properties of indirect stimulated emission.

I. INTRODUCTION

The optical properties of highly excited semiconductors are strongly influenced by many-particle effects.¹⁻³ The generation of a dense electron-hole system, e.g., by optical pumping, brings about significant modifications in the electronic band structure. Screening in the electron-hole system, i.e., the collective response of the system to interactions resulting from Coulomb and exchange effects, leads to a renormalization of the single-particle energies.¹⁻⁶ In particular, each carrier in the system repels all others with the same charge via the Coulomb force. This results in a local decrease of the average charge density at the position of any carrier, which can be described by an induced virtual charge of opposite sign. The repulsion process is counterbalanced by the buildup of this virtual charge such that each carrier sustains a free space around itself—the so-called correlation hole. A similar effect is induced by the Pauli exclusion principle which prohibits the fermions in the same spin state to occupy the same position. The spatial separation of the carriers is thus larger than expected classically leading to a reduction of the Coulomb repulsion. These rearrangements in the dense electron-hole system induced by correlation and exchange effects reduce the energy of the carriers significantly. The result is a narrowing of the band gaps in the highly excited semiconductor with respect to the unexcited case. The low-energy onset of intrinsic luminescence or gain is shifted to the red bearing important consequences for the performance of electro-

optic devices such as semiconductor lasers.⁷

A thorough understanding of these many-particle effects has been obtained for the case of a simple band structure with one minimum in the conduction band and one maximum in the valence band, including the modifications due to degeneracy and anisotropy of the band extrema.⁴⁻⁶ Such phenomena as band-gap renormalization (BGR),¹⁻¹¹ screening of the excitonic resonances by an excitonic gas or free carriers,^{1-3,12} the Mott transition from an excitonic gas to an electron-hole plasma (EHP),^{4,13} or the phase transition to an electron-hole liquid^{4,13,14} have been extensively investigated both theoretically and experimentally. An often applied approach to the treatment of the many-particle system is the random-phase approximation (RPA).^{1,2} The corrections to the single-particle self-energy here are splitted into two contributions: the correlation-hole and the screened-exchange terms. The latter terms takes into account that the exchange interaction is reduced because the Coulomb repulsion prohibits the close encounter of any two carriers with same charge, which is necessary for the Pauli principle to be invoked. Vashishta and Kalia (VK) demonstrated by applying a self-consistent mean-field theory to several model systems that the sum of the correlation and exchange energy can be approximated by a universal formula, once the self-energy corrections and the carrier density are expressed in reduced units of the excitonic rydberg and a normalized interparticle distance, respectively.^{5,6} This universal formula was experimentally proven to apply to nondrifting electron-hole plasmas

or liquids in nonpolar semiconductors like Si or GaAs,^{8,15} but has to be corrected for polaron effects in polar compounds like CdS.¹⁶

The description of many-particle effects in a dense EHP gets significantly more complicated, when not only the fundamental band gap but also gaps or subband transitions at higher energies are considered. Large efforts are actually taken nowadays to solve the problems of intersubband screening and exchange effects in two-dimensional (2D) systems (see, e.g., Refs. 17–20). We will focus in this paper on the many-particle interactions between inequivalent minima in bulk semiconductors. The main differences between the bulk and the 2D case lie for one in the fact that Coulomb screening is very inefficient in 2D.²¹ Further, interband exchange in 2D (Ref. 20) has to be considered between quantized levels of the same conduction-band minimum rather than minima at different points of the Brillouin zone as in the bulk case.

The treatment of the BGR in a multiple-valley situation in bulk material is essentially reduced to the correct evaluation of the electron-exchange effects.^{9–11} Based on the fact that exchange between carriers in minima at different points of the Brillouin zone is negligible,²² we develop a model which accounts for the exchange in each individual minimum of the conduction band. This model applies a simple formalism relying on the high-density limits of the many-body theories of Refs. 2, 5, 6, and 22. The population and renormalization of each gap are calculated self-consistently. This formalism does not require any many-particle calculations and is thus easily applicable for practical purposes. The main effect of a multivalley scenario as incorporated in this model is that different populations in the conduction-band minima due to the different effective masses lead to differential renormalizations of all minima.

The model system for our studies on band-gap renormalization is the semiconductor alloy $\text{Al}_x\text{Ga}_{1-x}\text{As}$. This material system is an extensively used compound in modern, fast semiconductor devices. It not only serves as a barrier material in GaAs/ $\text{Al}_x\text{Ga}_{1-x}\text{As}$ heterostructures, but is also currently exploited for laser and light-emitting diodes in the visible spectral range.^{23,24} We will show in the discussion below that the performance of these devices is strongly affected by the BGR. A most interesting feature of this material system is that a systematic change in the AlAs mole content x provides a tunability of the band structure. The nature of the fundamental band gap changes from direct to indirect at a crossover composition x_c where the X -point minima of the conduction band get lower in energy than the minimum at the Γ point.^{23,25} This most interesting property allows these minima as well as the L minima to be only slightly separated in energy for compositions close to x_c . Two typical configurations of the band structure close to the crossover are depicted in Fig. 1. It is easy to populate simultaneously the minima at different points in the Brillouin zone by optical pumping and thus to study the interaction between the inequivalent minima.

In this paper we want to review our studies on the BGR in $\text{Al}_x\text{Ga}_{1-x}\text{As}$, part of which have been previous-

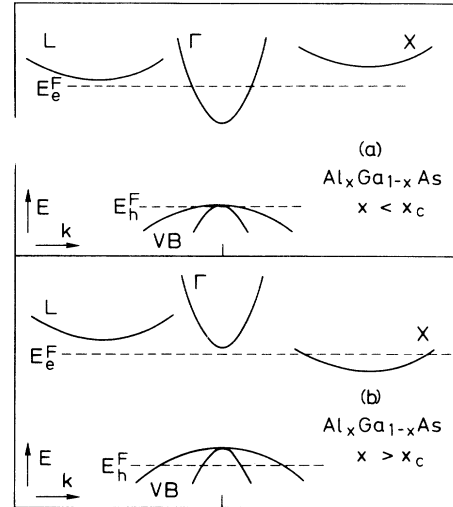


FIG. 1. Schematic picture of the band structure of (a) direct-band-gap and (b) indirect-band-gap $\text{Al}_x\text{Ga}_{1-x}\text{As}$ close to the crossover composition x_c . The positions of the quasi-Fermi levels are shown for typical excitation conditions. The higher threshold for the onset of stimulated emission in case (b) makes possible higher carrier densities [and thus a larger degeneracy of the valence-band (VB)].

ly published as short communications (Refs. 9–11). We will first give a description of the samples used, the method of picosecond photoluminescence, and how to extract the essential parameters for the study of BGR from a luminescence line-shape analysis (Sec. II). In Sec. III we will outline the theoretical model for BGR in a multivalley scenario. A description of the two-band model and the universal (VK) formula in Sec. III A will be followed by the extension to a multivalley model (Sec. III B). The extended model is first tested for the case of indirect band-gap $\text{Al}_x\text{Ga}_{1-x}\text{As}$, where the higher-energy Γ minimum is nearly empty and thus electron-exchange contributions to the BGR of the direct band gap are negligible. The influence of significant population of side valleys on the BGR of the fundamental gap is then demonstrated for direct band-gap $\text{Al}_x\text{Ga}_{1-x}\text{As}$. Section IV deals with the ordering of the conduction-band minima in highly excited $\text{Al}_x\text{Ga}_{1-x}\text{As}$ and its practical consequences. We will demonstrate a laser-induced change-over of a direct band-gap semiconductor material to an indirect band-gap one as a result of the differential BGR of the gaps (Sec. IV A) and prove further minima crossings by the properties of stimulated-emission processes (Secs. IV A and IV B). We will finally summarize in Sec. V.

II. EXPERIMENTAL IMPLEMENTATIONS

A. Samples and experimental setup

The investigations of the BGR in multivalley configurations were performed on thin (1–2 μm) epitaxial

layers of $\text{Al}_x\text{Ga}_{1-x}\text{As}$ with x values close to the crossover point. The samples were grown by either molecular-beam epitaxy (MBE) or liquid-phase epitaxy (LPE) on a high x value ($x \approx 0.70$) $\text{Al}_x\text{Ga}_{1-x}\text{As}$ barrier layer of $1 \mu\text{m}$ thickness on a semiinsulating GaAs substrate. The barrier layer serves two purposes: first it ensures a high quality of the active layer by prohibiting diffusion of defects from the substrate. Second, the barrier layer provides strong carrier confinement for the holes in the active layer due to the large valence-band offset.²⁶ The offset in the conduction band is actually negative between active layers close to x_c and $x = 0.70$ barrier layers.²⁶ This effect is, however, compensated by the strong renormalization of the minima in the highly excited active layer and by a self-confinement of the electron-hole plasma in indirect band-gap $\text{Al}_x\text{Ga}_{1-x}\text{As}$.¹⁴ The MBE grown samples had an additional few 100-Å-thick GaAs cap layer to prevent oxidation of the sample surface. No significant differences in experimental results were found between the LPE and MBE-grown materials under high-excitation conditions.

The calibration of the AlAs-mole fraction x of our samples was performed using optical methods. We determined the energy of the exciton resonance from low-excitation time-integrated photoluminescence and from photoluminescence excitation spectroscopy (compare also Fig. 10) at 5-K lattice temperature. One sample, the optical properties of which characterized it as being just below the crossover composition, was used as a reference sample. Its x value was determined from high-resolution x-ray diffraction to be $x = 0.423$, which is in close agreement with the low-temperature data of Wolford *et al.*²⁵ The relative x values of the other samples and the positions of the unrenormalized band gaps were then calibrated according to the data of Ref. 25. The samples were mounted to a cold finger in a He cryostat and kept at a lattice temperature of 5 K unless stated otherwise.

A dense EHP is generated in the active layer of the samples by optical excitation with a picosecond pulse (25 ps full width at half maximum) at 532 nm from a frequency doubled, amplified, actively and passively mode-locked Nd:YAG laser. The excitation-spot size on the sample is about $800 \mu\text{m}$ and excitation fluences of up to $80 \text{ mJ}/\text{cm}^2$ are used. Only the center portion of the excited area is imaged to the entrance slit of an 0.25-m spectrometer to ensure homogeneous excitation conditions. A single-shot streak camera is connected to the exit of the spectrometer. By use of a 2D read-out system the luminescence signal from the bimolecular electron-hole recombination in the EHP is detected simultaneously dispersed spectrally and temporally with resolutions of 1 meV and 30 ps, respectively. Additional experiments at lower excitation levels were performed employing a synchronously pumped dye laser and Synchroscan streak camera with a temporal resolution of 10 ps (see also Refs. 14 and 27).

B. Time-resolved electron-hole plasma luminescence and line-shape analysis

The picosecond temporal resolution of our experiments is essential to identify the observed luminescence bands.

First, we are able to separate the recombination processes involving different conduction-band minima. This is important in the case of indirect band-gap materials when the generation of the EHP occurs mainly via direct absorption. The electrons excited typically with some excess energy in the central Γ valley are transferred into the sidevalleys at the X or L points on a subpicosecond time scale. This intervalley scattering involves in semiconductor alloys not only the interaction with optical and/or acoustic phonons, but also very efficiently the scattering via the alloy-disorder potential.^{27,28} But, the intravalley relaxation of the electrons within the central valley occurs on an even faster time scale. This fast process which results mainly from electron-electron scattering is reflected in the observation of direct luminescence in the indirect band-gap materials. This luminescence is thus detected not close to the excitation photon energy, but rather at photon energies corresponding to the direct gap in this highly excited materials. A significant number of the electrons are able to recombine with holes in the valence band before they had the chance to be transferred to the side valleys. This luminescence band (dashed line in Fig. 2) is easily identified from its temporal evolution which just follows the temporal shape of the excitation pulse. The indirect emission (in our experiments involving mainly the X minima, see solid line in Fig. 2), however, has typical decay times in the order of 600 ps. The distinction between direct and indirect recombination is thus straightforward.²⁹

The second important conclusion from the temporal development of the luminescence is the attribution of the low-energy bands in Fig. 2 (dotted and dash-dotted lines) to recombination involving the same conduction-band minima. The temporal behavior of the three partially overlapping bands is found to be identical within the luminescence decay time. Elaborate investigations of the relative strength of these bands especially as a function of energetical separation between Γ and X minima led to the unambiguous identification of these bands: a zero-

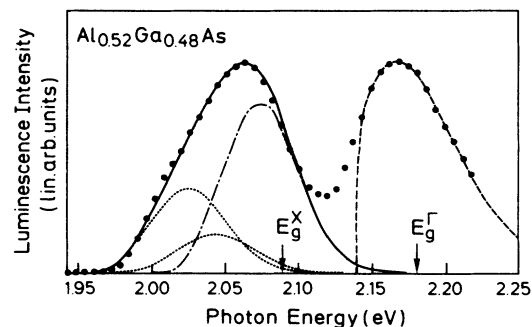


FIG. 2. Luminescence signal (dots) of an indirect band-gap sample while the picosecond excitation pulse at 2.33 eV ($F = 8 \text{ mJ}/\text{cm}^2$) is present. The indirect emission is fitted (solid line) by a superposition of a zero-phonon line (dashed-dotted) and two phonon sidebands (dotted). The dashed line is a fit to the direct recombination signal neglecting the broadening at the low-energy tail. The arrows mark the unrenormalized direct and indirect band gaps.

phonon line resulting from the band mixing via the alloy disorder and two phonon sidebands involving the emission of a GaAs-like or an AlAs-like longitudinal-optical (LO) zone-edge phonon.²⁷

Finally, our temporally and spectrally resolved luminescence experiment allows us to identify stimulated emission processes from their thresholdlike occurrence, their short temporal duration (mostly following the temporal shape of the laser pulse), in combination with their narrow spectral shape and their spectral position at the renormalized gap.^{30,31} It is most important that very efficient stimulated recombination of holes with electrons in the side minima at the X and L points occurs in the alloy $\text{Al}_x\text{Ga}_{1-x}\text{As}$ with indirect fundamental gaps. We will exploit these stimulated emission processes to discuss the crossing of direct and indirect gaps in Sec. IV. The main bulk of the analysis, especially when a luminescence-line-shape analysis is used, is performed, however, for conditions well below the onset of stimulated emission.

The experimental data for the renormalized band gaps and the carrier densities, which will be compared to the results of the many-particle theories,^{2,5,6,22} are extracted from modeling of the luminescence line shape. The case of indirect band-gap $\text{Al}_x\text{Ga}_{1-x}\text{As}$ is demonstrated in Fig. 2. The modeling of the indirect recombination bands requires the superposition of a zero-phonon line with two phonon sidebands.²⁷ The intensity profile $I(\hbar\omega)$ of the zero-phonon line is given by³²

$$I(\hbar\omega) \propto \hbar\omega \int_0^{\hbar\omega - E'_g} E'^{1/2} [\hbar\omega - E - E'_g(n)]^{1/2} \times f_e(E_e - E'_g, n, T) f_h(E_h, n, T) dE, \quad (1)$$

where E'_g denotes the renormalized energy of the fundamental gap, $f_{e,h}(E, n, T)$ are the Fermi functions for electrons and holes, respectively, and the electron and hole energies, E_e and E_h , fulfill $E_e + E_h = \hbar\omega$. The fit parameters are the carrier density n , the renormalized gap E'_g , and the carrier temperature T , which can be assumed to be equal for electrons and holes but always deviates from the lattice temperature due to the excess energy acquired during the laser excitation.

The quasi-Fermi energies of electrons and holes $E_{e,h}^F$ are implicitly given by³³

$$n_{e,h} = N_{e,h}^c F_{1/2}(\eta_{e,h}), \quad (2)$$

where $\eta_{e,h} = E_{e,h}^F / k_B T$ are the reduced quasi-Fermi-levels, the effective density of states $N_{e,h}^c$ is defined by

$$N_{e,h}^c = 2 \left[\frac{2\pi m_{e,h} k_B T}{h^2} \right]^{3/2}, \quad (3)$$

and $F_{1/2}(\eta_{e,h})$ is a Fermi-Dirac integral, k_B the Boltzmann constant, h Planck's constant, and $m_{e,h}$ the density-of-states effective masses as defined below. The inversion of Eq. (2) is done using the approximation of Aguilera-Navarro, Estevez, and Millar³⁴ which is applicable even for very high carrier densities ($0 \leq n/N^c \leq 170$):

$$\eta_{e,h} = \ln \left[\frac{n}{N_{e,h}^c} \right] + K_1 \ln \left[K_2 \frac{n}{N_{e,h}^c} + K_3 \right] + K_4 \frac{n}{N_{e,h}^c} + K_5, \quad (4)$$

with the constants K_1, \dots, K_5 given in Ref. 34. With the reduced quasi-Fermi-levels for a given set of n , T , and E'_g one can now calculate the Fermi functions $f_{e,h}$.

In a multiple-valley scenario like in $\text{Al}_x\text{Ga}_{1-x}\text{As}$ close to x_c one has to account for the carrier distribution among several inequivalent valleys by calculating the total electron density from

$$n_e = n_e^\Gamma + n_e^X + n_e^L, \quad (5)$$

and assuming a common quasi-Fermi-level for all minima, i.e.,

$$\eta_e^X = \eta_e^\Gamma - \frac{E_g'^X - E_g'^\Gamma}{k_B T} \quad (6)$$

and

$$\eta_e^L = \eta_e^\Gamma - \frac{E_g'^L - E_g'^\Gamma}{k_B T}. \quad (7)$$

The masses for the X and L minima which are used in Eq. (3) are the combined density-of-states masses for three or four equivalent valleys, respectively (see Table I). The renormalized gaps $E_g'^\Gamma$, $E_g'^X$, and $E_g'^L$ and the electron densities in the corresponding minima are calculated self-consistently, as explained in Sec. III B. We further account for the nonparabolicity of the central minimum by replacing N_{np}^c for N_e^c in Eq. (3) with³³

$$N_{np}^c = N_e^c \left[1 - \frac{15\alpha k_B T}{4E_g^\Gamma} \frac{F_{3/2}(\eta_e^\Gamma)}{F_{1/2}(\eta_e^\Gamma)} \right]. \quad (8)$$

The Fermi-Dirac integrals are approximated according to Aymerich-Humet, Serra-Mestves, and Millan,³⁵ and the nonparabolicity coefficient α is given by³³

$$\alpha = - \frac{(1 - m_e/m_0)^2 (3E_g^2 + 4E_g \Delta_{s.o.} + 2\Delta_{s.o.}^2)}{(E_g + \Delta_{s.o.})(3E_g + 2\Delta_{s.o.})}. \quad (9)$$

The x -value-dependent spin-orbit splitting $\Delta_{s.o.}$ and the direct gaps are taken from Table I.

The hole quasi-Fermi-level is determined from $n_h = n_e$ and using an approximation of the valence-band structure close to the Γ point by a single parabolic band with a density-of-states effective mass m_h of

$$m_h = (m_{lh}^{3/2} + m_{hh}^{3/2})^{2/3}, \quad (10)$$

where $m_{lh}(x)$ and $m_{hh}(x)$ are the composition dependent light- and heavy-hole masses.

The line shape of the phonon sidebands is identical to the zero-phonon line except for being shifted by the energy of the zone-edge GaAs-like or AlAs-like LO phonons and being normalized in height to the experimental spectrum. We do not consider any final state damping resulting from fast intraband interaction in these line-shape fits. This damping is usually treated in the form of the

Landsberg broadening of the actual line shape, which is introduced only phenomenologically.³⁶ Its inclusion in the fit would only slightly change the extracted parameters, especially in the case of relaxed momentum conservation. All material parameters used in these calculations are listed in Table I.

On first sight the fit might appear to be somewhat arbitrary, because all bands are rather broad in the case of a dense EHP. The fit procedure was, however, extensively tested in the case of the electron-hole droplet phase, which is observed in this material system when the temperature of the plasma is below the critical temperature $T_c = 34$ K. In this liquid phase as well as in the excitonic gas the individual contributions to the overall line shape are clearly separated and the energies of the LO phonons can be determined accurately.^{27,41} The relative intensities of the zero-phonon emission and the sidebands in the plasma luminescence (Fig. 2) compare well to the ratios found for the excitonic luminescence for the same composition. Our investigations have to be performed in the EHP phase in order to get detailed information on the BGR in an extended density range. The reason is that the density in the droplet system is rather insensitive to the excitation conditions and limited to a small density range around $4 \times 10^{18} \text{ cm}^{-3}$.¹⁴ The theoretical treatment of the BGR is not affected by the actual phase of the dense electron-hole system.

The shape of the direct emission in this indirect-band-gap case is largely influenced by the transient state of the electrons in the central valley. The large extension of this band on the high-energy side reflects the rather high carrier temperature in the electron system of the Γ minimum. Cooling of the carrier distribution by emission of optical phonons is slow in comparison to the intraband thermalization via electron-electron scattering and the interband transfer assisted by optical phonons and alloy disorder. Please note that cooling of the carriers in the side valleys is in comparison much more efficient due to the fact that a buildup of nonequilibrium phonons is not important in minima with high effective mass and large anisotropy.⁴² The electrons in the Γ minimum do not have time to thermalize with the carriers which have already scattered into the side valleys. The carrier temperature of the Γ electrons is thus significantly higher than that of the X electrons.

The second consequence of the rapid interband transfer of the electrons is the large difference in the relative carrier densities in the minima at Γ and X points. The electrons are swept out of a central valley, where they are predominantly generated, into the sidevalleys and accumulate there. The quasi-Fermi-level of the electrons is in any case far below the renormalized Γ minimum. The direct emission thus reflects a rather small carrier density in contrast to the indirect emission.

TABLE I. Composition dependence of the material parameters.

Parameter	Composition dependence	Reference
E_g^Γ (300 K)	$(1.424 + 1.247x) \text{ eV}$ $0 \leq x \leq 0.45$	23
	$[1.424 + 1.247x + 1.147(x - 0.45)^2] \text{ eV}$ $0.45 \leq x \leq 1$	23
E_g^L (300 K)	$(1.708 + 0.642x) \text{ eV}$	23
E_g^X (300 K)	$(1.900 + 0.125x + 0.143x^2) \text{ eV}$	23
E_g^Γ, E_g^L, E_g^X (5 K)	According to Fig. 2 in Ref. 25	25
$\Delta_{s.o.}$	$(0.34 - 0.065x) \text{ eV}$	40
m_e^Γ	$(0.067 + 0.083x)m_0$	23
m_e^L	$(0.55 + 0.12x)m_0$	23
m_e^X	$(0.85 - 0.07x)m_0$	23
m_l^X	$(1.9 - 0.34x)m_0$	33,37
m_l^X	$0.19m_0$	33,38
m_l^L	$1.9m_0$	33,39
m_l^L	$(0.076 + 0.02x)m_0$	33,39
m_{hh}	$(0.51 + 0.25x)m_0$	33
m_{lh}	$(0.082 + 0.068x)m_0$	40
ϵ_s	$12.6 - 2.5x$	33
$Ry^*(\Gamma)$	6.5 meV ($x=0.38$) 7.5 meV ($x=0.52$)	
$Ry^*(X)$	11.0 meV ($x=0.38$) 12.1 meV ($x=0.52$)	
$Ry^*(L)$	7.0 meV ($x=0.38$) 7.5 meV ($x=0.52$)	
E_{LO}^{GaAs}	29 meV ($x=0.42$) 30 meV ($x=0.52$)	41
E_{LO}^{AlAs}	45 meV ($x=0.42$) 47 meV ($x=0.52$)	41
Zone-edge phonons		

The extremely fast intraband thermalization of the electrons in the Γ valley enables us to determine the energetic position of the direct gap. This determination is, however, blurred to some extent by the broadening of electron states due to the short lifetime and the already discussed Landsberg broadening. The broadening is in the order of 3 meV resulting from an intervalley transfer time of about 200 fs.²⁷ The final-state damping will mainly produce a tailing of the line shape to the low-energy side of a few meV.⁸ It is possible now to include the Landsberg broadening into the line-shape analysis. This will give enough fit parameters to reproduce the overall line shape. The analytical form of this broadening is, however, arbitrarily chosen and does not directly compare to the broadening expected from many-body theories.⁴³ The dashed line in Fig. 2 indicates the expected line shape of the direct recombination in a k -conserving model without broadening:

$$I(\hbar\omega) \propto \hbar\omega(\hbar\omega - E_g^{\prime\Gamma})^{1/2} f_e(E_e - E_g^{\prime\Gamma}, n, T) f_h(E_h, n, T). \quad (11)$$

In the case of direct emission in indirect band-gap $\text{Al}_x\text{Ga}_{1-x}\text{As}$ this line-shape analysis suffices to determine the position of the renormalized direct gap with an uncertainty of maximum 10 meV. This uncertainty is in any case much smaller than the effects of reduction in the BGR as will be discussed below. The temperature used for the line-shape fit is in the order of 100–200 K and reflects the transient behavior of the electrons and the nonequilibrium with the carriers in the sidevalleys.

The applicability of this simple line-shape analysis can be demonstrated for the case of direct-band-gap materials, where the carrier distribution and temperature are better defined. A line-shape fit as used by Capizzi *et al.* (Ref. 8), which includes an explicit evaluation of the final-state damping in RPA, is able to reproduce the full line shape. An extensive treatment of the emission shape in RPA is given by Selloni, Modesti, and Capizzi.⁴⁴ This approach eliminates the renormalized gap as a fit param-

eter, but rather calculates this value self-consistently. This elaborate model gives similar results as Ref. 8. For practical purposes it is, however, only necessary to determine the quantities n , T , and E_g^{\prime} , but it is not essential to fully reproduce the low-energy tail of the luminescence. We demonstrate this in Fig. 3 where we directly compare an analysis with and without a Landsberg-type broadening of a luminescence spectrum taken from Ref. 8. We find that, when we allow for deviations at the low-energy tail and concentrate on the rest of the spectrum, we can extract the necessary fit parameters with negligible deviations from the values extracted in Ref. 8 for the same spectrum.

III. MULTIVALLEY MODEL FOR BAND-GAP RENORMALIZATION

A. The two-band model and the universal formula

We will now develop a model to describe the BGR in the scenario of a semiconductor with various inequivalent minima in the conduction band. This model especially answers questions like how do carriers residing in one minimum interact with the carriers in other minima and do minima which are highly above the quasi-Fermi energy and thus essentially empty still renormalize under high-excitation conditions. We will, in the following, first deal with the renormalization of the fundamental gap for the condition that the population of higher-energy minima is negligible, and then expand the here used formalism to the multivalley situation.

The energy of electrons or holes in an electron-hole plasma $E_{e,h}(\mathbf{k})$ is described by the sum of their respective kinetic energies and the real part of their single-particle energies $\Sigma_{e,h}$:^{1,2}

$$E_{e,h}(\mathbf{k}) = \frac{\hbar^2 k^2}{2m_{e,h}} + \text{Re}\Sigma_{e,h}(\mathbf{k}, E_{e,h}(\mathbf{k})) \quad (12)$$

with \mathbf{k} being the wave vector and m the effective mass of the electrons or holes. This single-particle energy is given in RPA by the convolution of the single-particle Green's function and the dynamically screened Coulomb interaction typically treated in a single plasmon pole approximation. The Green's function incorporates here the full characteristics of the band structure. It was shown that the self-energy $\Sigma(\mathbf{k}, E(\mathbf{k}))$ is nearly independent of the value and direction of \mathbf{k} and $E(\mathbf{k})$ due to the local nature of the screened interactions. The consequence is a nearly rigid shift of the band structure in the region of the occupied states within one band extremum and an only small renormalization of the effective masses.² Please note that this rigidity does not apply to the full band structure, i.e., unoccupied states, extrema at different points of the Brillouin zone, or different 2D subbands are not shifted rigidly as will be demonstrated below. The rigidity within each band extremum, however, leads to the fact that the band gap and the chemical potential (i.e., the sum of the quasi-Fermi energies) are shifted by the same amount. The BGR ΔE_g^{\prime} is thus directly related to the renormalized chemical potential μ :

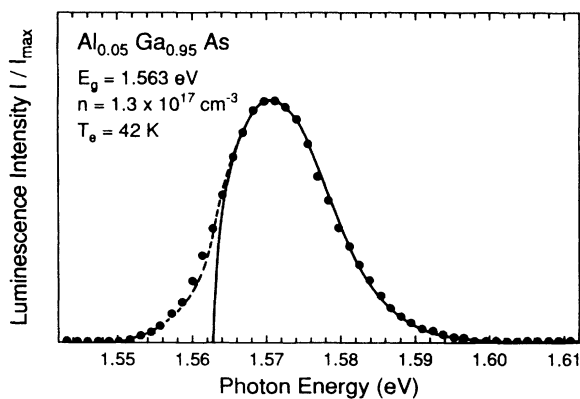


FIG. 3. Luminescence signal (dotted line) of a direct band-gap sample taken from Fig. 4 of Ref. 8 and line-shape fits with (dashed line) and without (solid line) inclusion of a Landsberg-type broadening. The fit parameters for both fits are identical and agree well with the parameters used in Ref. 8.

$$\mu = E_F^e + E_F^h + \Sigma_e + \Sigma_h \quad (13)$$

by the contributions of the electron and hole self energies:

$$\Delta E_g = \Sigma_e + \Sigma_h . \quad (14)$$

It is more convenient to write the BGR as a function of the excited carrier density n and to combine the self-energy terms, which describe the effects of correlation and exchange in the EHP, in the exchange-correlation energy E_{xc} .¹⁻⁶ The definition of the chemical potential as function of density leads to the formula for the BGR of the fundamental gap:

$$\Delta E_g = E_{xc} + n \frac{\partial E_{xc}}{\partial n} . \quad (15)$$

The exchange-correlation energy is typically split into a Coulomb hole E_{Ch} and a screened-exchange term E_{sx} for further theoretical treatment:^{1,2}

$$E_{xc} = E_{Ch} + E_{sx} . \quad (16)$$

The former term incorporates the correlation effects in the EHP, while the latter describes the results of the Pauli-exclusion principle. The screened exchange takes into account that this interaction is reduced by the fact that the Coulomb repulsion prevents the carriers of the same charge to approach each other closely enough for the short-range exchange to be efficient.

A quite remarkable finding is that the sum of correlation and exchange energies is nearly independent of band-structure details like the electron-hole mass ratio, the degeneracy, and the anisotropy of band extrema. This was shown by Vashishta and Kalia which applied a self-consistent mean-field theory to various semiconductor systems.^{5,6} The changes in one of the contributions to the exchange-correlation energy is always compensated by the other, a tendency which also applies to some extent to the temperature dependence of this energy.² This property leads to the possibility to describe E_{xc} in a universal formula applicable to all semiconductors with small polar coupling once the energy and the carrier density are expressed in reduced units of the excitonic rydberg Ry^* and a normalized interparticle distance r_s , respectively:

$$1 Ry^* = \frac{e^4 m_x}{(4\pi\epsilon_s)^2 2\hbar^2} \quad (17)$$

$$r_s = \left[\frac{3}{4\pi n} \right]^{1/3} \frac{1}{a_B} , \quad (18)$$

with e being the elementary charge, m_x the reduced excitonic mass, ϵ_s the static dielectric constant, and a_B the excitonic Bohr radius. This normalized distance is equal to one when the average volume allotted to each electron-hole pair in the plasma equals the volume of the exciton. Please note that the Mott transition from an excitonic gas to an EHP occurs at an r_s of 3.4 at 30 K. The universal formula now reads^{5,6}

$$E_{xc}(r_s) = \frac{a + br_s}{c + dr_s + r_s^2} Ry^* \quad (19)$$

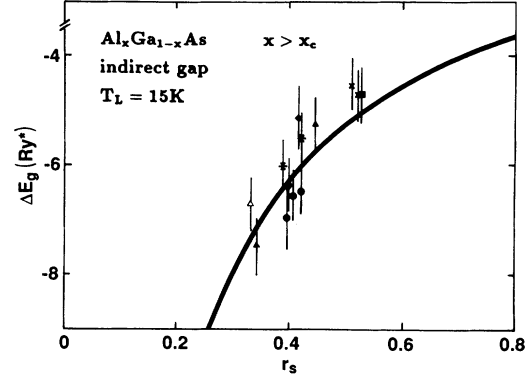


FIG. 4. Band-gap renormalization of the fundamental gap in indirect-band-gap $Al_xGa_{1-x}As$. The different symbols used for the data points stand for results taken in seven different samples with x values between 0.49 and 0.55. The solid line represents the universal formula [Eqs. (15) and (19)].

with the material-independent constants $a = -4.8316$, $b = -5.0879$, $c = 0.0152$, and $d = 3.0426$. This simple expression only depends on one parameter, namely, the carrier density in reduced units.

The applicability of this formula was tested in several semiconductor materials like Si, Ge, or GaAs.^{8,15} Only in polar compounds like II-VI semiconductors this formula has to be corrected for polaron effects which further reduce the band gap and stabilize the EHP phase.¹⁶ We will demonstrate in the following the range of applicability of this approach to the $Al_xGa_{1-x}As$ system and the necessary extensions. We will start with the case of indirect band-gap $Al_xGa_{1-x}As$, where the population of the minima at the Γ and L points are negligible. The case of direct band-gap $Al_xGa_{1-x}As$ will be discussed in Sec. III B.

The renormalization of the indirect fundamental gap is determined from the luminescence signal of seven different samples. Their x values are between 0.49 and 0.55 to ensure that only the X minima are populated. The carrier densities range between 10^{19} cm^{-3} and $3 \times 10^{19} \text{ cm}^{-3}$. The BGR is plotted in Fig. 4 in reduced units as a function of the normalized interparticle distance. The experimental data are in very good agreement with the universal behavior given in Eq. (19) (solid line in Fig. 4). We want to emphasize again that the theoretical model contains no adjustable parameters. Excellent agreement is further found in samples just above the direct-to-indirect crossover, where the carrier density is between $4 \times 10^{18} \text{ cm}^{-3}$ and $8 \times 10^{18} \text{ cm}^{-3}$ to avoid significant population of the Γ and L minima (see Ref. 14). The VK two-band model thus describes well the BGR of the fundamental gap, when higher-energy minima are essentially empty.

B. The extension to a multivalley model

The observation of luminescence involving electrons in the central minimum gives the possibility to study the renormalization of the direct gap in indirect $Al_xGa_{1-x}As$. This gap extends between the top of the highly populated

valence band and the bottom of the only slightly occupied Γ minimum. Accounting for the fast transfer of the electrons into the X minima we can assume the Γ minimum to be essentially empty in comparison to the heavily populated X minima. The gap narrowing of the direct gap is depicted in Fig. 5 using the direct-band-gap parameters to determine the reduced units. It is important to note that the narrowing of the direct gap amounts to 25–40 meV, while the fundamental indirect gap is reduced by 60–90 meV as deduced from the same luminescence spectra. The immediate conclusion is that the direct gap in indirect band-gap materials renormalizes but by a much smaller amount than the fundamental gap.

The actual amount of renormalization of the direct gap can be calculated from a multivalley expansion of the simple VK universal formula. The universal formula is again plotted as a solid line in Fig. 5. This unmodified version of the model overestimates the renormalization by a factor of 2, because it assumes all electrons to be in the central valley, which is of course not the case. One expects the few electrons in the Γ minimum to have still Coulomb interaction with the majority of electrons residing in the X minima. The exchange interaction between electrons at different points of the Brillouin zone is expected to be negligible, i.e., the exchange interaction is restricted essentially to electrons within the same valley.²² The contribution of the holes to the narrowing of the direct gap is, however, the same as in the case of the

indirect gap. These arguments directly lead to the model for the renormalization of the direct gap. We start from the universal formula in Eq. (19) and simply subtract the exchange interaction between the electrons, which is the only contribution missing:

$$\Delta E_g^\Gamma = E_{xc} + n \frac{\partial E_{xc}}{\partial n} - \left[E_x^e + n \frac{\partial E_x^e}{\partial n} \right]. \quad (20)$$

In the calculation of the electron-exchange energy E_x^e we use the unscreened interaction, which is given by

$$E_x^e = \frac{-0.916\phi(\rho_e)}{r_s v_e^{1/3}}, \quad (21)$$

where v_e is the valley degeneracy factor, and ϕ describes the valley anisotropy as a function of the ratio ρ_e of the transverse and longitudinal effective masses:²²

$$\phi(\rho) = \rho^{1/6} \frac{\sin^{-1}[(1-\rho)^{1/2}]}{(1-\rho)^{1/2}} \quad \rho < 1. \quad (22)$$

In the case of the Γ minimum both, ρ_e and v_e are unity which largely simplifies Eq. (21).

The justification of this ansatz is deduced from the experimental observation that the BGR is reduced by 50% only due to the missing electron exchange. This finding demonstrates that the electron-correlation effects give only a minor contribution to the renormalization for these very high carrier densities. It is actually expected from theory that the BGR should be essentially determined by the exchange effects in the limit of high densities.² This behavior has an intuitive explanation: The carriers have no space to be repelled from each other at high carrier densities or r_s values much smaller than one. The reduction of the exchange interaction by the Coulomb repulsion is thus increasingly compensated. The result of the calculation using the ansatz of Eqs. (20) and (21) is shown as a dashed line in Fig. 5. Again, we find an excellent agreement between the experimental data and our model.

We can conclude at this point that our simple approach to the many-particle effects is able to explain the renormalization of both the highly populated lowest as well as the sparsely populated higher minima in the limit of high total carrier densities. The fundamental gap renormalizes according to the two-band VK model. The higher-energy gaps still narrow considerably, because of the strong renormalization of the highly populated valence band. The contribution of the nearly empty conduction-band minimum to the gap reduction is minimal, because the correlation effects are weak and the electron-exchange contribution is negligible. This situation is however different in the low-density limit: In the case of the ionization of direct exciton in Ge, the Coulomb screening by electrons in the L minima was found to contribute significantly to the BGR of the direct gap.⁴⁵

The treatment of the renormalization gets more complex when the higher-energy minima of the conduction band are also significantly populated due to a small energetic separation between the minima or due to high car-

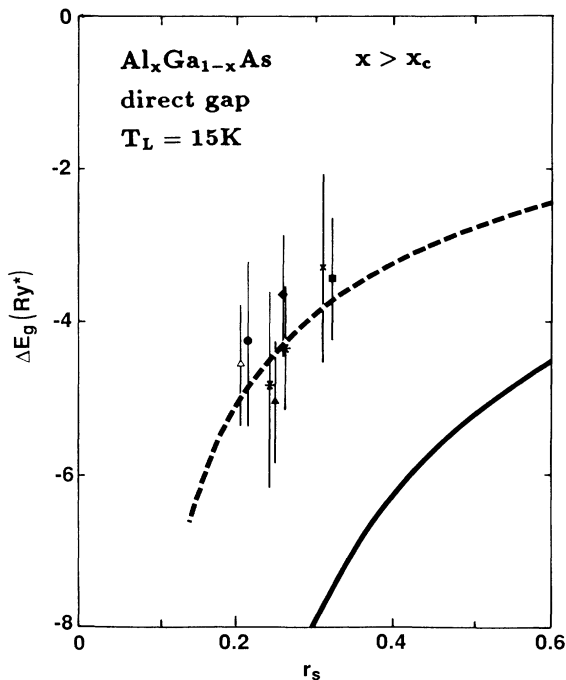


FIG. 5. Renormalization of the higher-energy direct gap in indirect-band-gap $\text{Al}_x\text{Ga}_{1-x}\text{As}$ extracted from the same spectra as used for Fig. 4. The choice of symbols for the data points is the same as in Fig. 4. The solid line again stands for the universal formula, while the dashed curve is corrected for the electron-exchange contribution to the BGR according to Eq. (20).

rier temperature. We have to extend our model here for the inclusion of the exchange effects within each conduction-band minimum and for a self-consistent determination of the population and renormalization of each valley. The model will be applied to direct band-gap $\text{Al}_x\text{Ga}_{1-x}\text{As}$ in various valley configurations.

The self-consistent multivalley model is based on the above demonstrated effect that the electron-exchange contribution to the BGR only results from interaction within the same valley. When the electrons are distributed among several nonequivalent minima, then only the density in each minimum is accounted for in the calculation of E_x^e . We again start the calculation by determining the BGR for the case when all electrons would be in the same minimum. This automatically takes care of the contribution of the hole interactions to the BGR of each gap. We then subtract the full electron-exchange contribution from the BGR according to Eq. (20) and just add the amount of $[E_x^e + n_v(\partial E_x^e/\partial n_v)]$ resulting from the actual population n_v in each minimum. Here, the anisotropy and degeneracy of the X and L minima have to be accounted for [see Eq. (22)]. We again assume that the modifications of the correlation energy are small when the electrons are distributed among various valleys and not situated in one minimum, because the correlation energy is a small contribution at high overall densities anyway.

The population of each conduction-band minimum is given by the Fermi function, the density of states in each valley, and the relative energy position of the minima. This relative position is, however, a direct function of the density-induced renormalization of each minimum. The calculation of the renormalization and population of each minimum thus requires a self-consistent treatment. We start in our calculations with fixed carrier densities and temperatures, and literature values for the unrenormalized gaps. The electrons are distributed among the valleys according to the Fermi function. We then determine the renormalization of each minimum induced by its population. The rearrangement of the relative energy separations between the minima now requires a redistribution of the electrons among the valleys according to the Fermi function and a subsequent redetermination of each renormalization. This procedure is continued until convergence is reached.

We will now describe how to apply this model to the case of direct-band-gap $\text{Al}_x\text{Ga}_{1-x}\text{As}$. Here, the self-consistent treatment of population and renormalization has to be included into the analysis of luminescence line shapes. This requirement can be demonstrated by the discussion of some earlier measurements of BGR in this material system. Close to the crossover composition, an enhancement of the renormalization of the fundamental gap was reported.^{8,9} The carrier density or the normalized interparticle distance, respectively, needed for the comparison of the gap shrinkage to the VK universal formula was taken from a line-shape analysis of the direct EHP luminescence. Such a line-shape analysis is, however, not valid when the populations of the higher-energetic conduction-band minima at the X and L points are neglected. These populations are not directly accessible

to the luminescence experiment, because a radiative recombination of these electrons with holes in the valence band has to proceed via an intermediate state in the Γ valley. The time scale for relaxation within the central valley by intraband scattering is, however, much shorter than the recombination time, which suppresses a detectable contribution of indirect recombination to the overall luminescence. This has some important consequences: first, the overall carrier density is larger than the density determined from the line-shape fits, because the direct emission signal is only determined by the difference between the bottom of the Γ minimum and the quasi-Fermi-level of the electrons. The carrier distribution in the valence band is only slightly degenerate, if at all, and the difference between the top of the valence band and the quasi-Fermi-level of the holes does not significantly contribute to the width of the direct luminescence [compare Fig. 1(a)]. The density determined from the fit thus only represents the density in the central valley. Our self-consistent calculations show that the overall density, and thus also the hole density, can be higher by a factor of 2 than the density in the Γ minimum. We will show in the following that this is the reason for the alleged enhancement of the renormalization in $\text{Al}_x\text{Ga}_{1-x}\text{As}$ close to the crossover composition.

A line-shape analysis of the direct emission has to include the population of the side valleys and the correct hole density. We incorporate our self-consistent model into the line-shape fits of Sec. II B in the following way: The start parameters density and carrier temperature are determined from a fit to the spectrum. Then we calculate the correct positions and populations of all minima and the valence band with the self-consistent routine. The fit is then repeated using now the calculated band-gap energies rather than the literature values. The newly determined n and T are the input of the next self-consistent calculation. This procedure is again repeated until convergence is achieved.

The first test of our multivalley model is the case of low population in the higher-energy minima. In this scenario the universal formula has to be recovered. We show two examples here: $\text{Al}_{0.23}\text{Ga}_{0.77}\text{As}$, which is far from the crossover composition, and GaAs close to the crossover point as a result of high hydrostatic pressure (Figs. 6 and 7). In the case of $\text{Al}_{0.23}\text{Ga}_{0.77}\text{As}$, the sidevalleys at the X and L points are so high in energy that their population at low temperature is negligible in the density range under consideration. In the case of GaAs under high hydrostatic pressure, only the X minima have to be considered. But their population is also negligible at 5 K for pressures well below the crossover pressure (42 kbar). The multivalley model reproduces in both situations the universal formula, whose validity is proven by the excellent agreement with the experimentally determined renormalizations.

We now apply our model to the experimental data in $\text{Al}_x\text{Ga}_{1-x}\text{As}$ just below the crossover composition as reported by Capizzi *et al.*⁸ The renormalization strongly deviates from the simple VK model as is shown in Fig. 8. This deviation is observed at high carrier densities for x values exceeding 0.30 and continuously increases towards

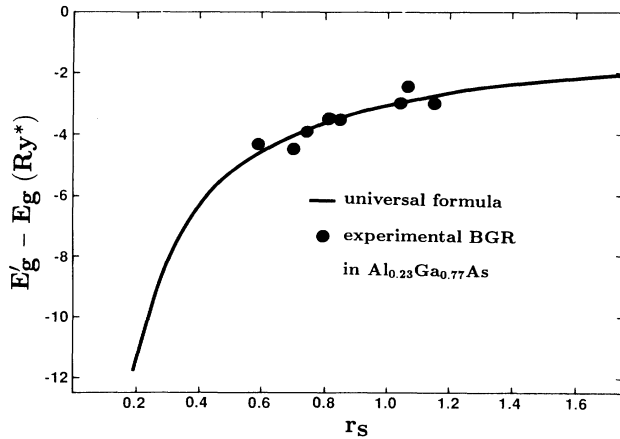


FIG. 6. Band-gap renormalization in a direct-band-gap $\text{Al}_x\text{Ga}_{1-x}\text{As}$ sample at $T_L = 15$ K for a composition, where the population of side valleys is negligible.

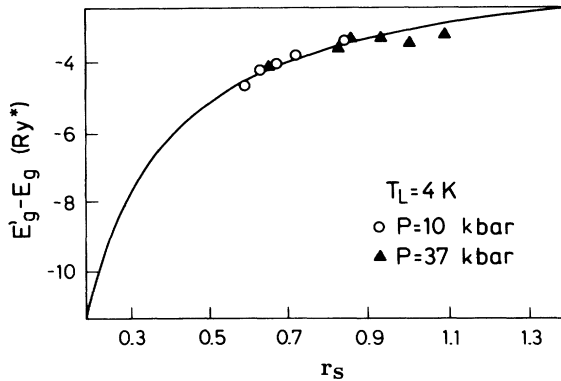


FIG. 7. Gap narrowing in GaAs under hydrostatic pressure. Experimental conditions are such that the population of the X valley is insignificant.

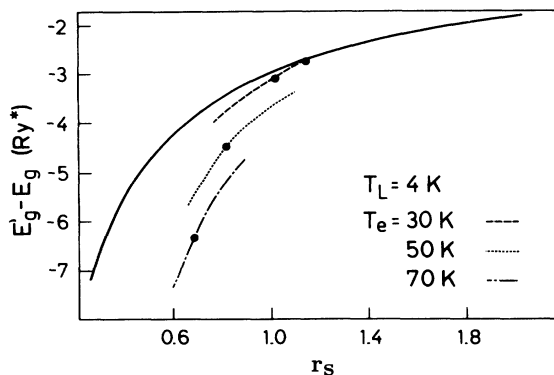


FIG. 8. Deviation of the experimental band-gap shift from the universal formula (solid line) in direct-band-gap $\text{Al}_x\text{Ga}_{1-x}\text{As}$ close to the crossover composition. Data points are taken from Ref. 8, which gives an x value of 0.42 for this sample. A comparison of the luminescence spectra to the spectra taken in our samples results in a composition of $x = 0.39$ in our calibration. The dashed, dotted, and dashed-dotted lines are calculated using the multivalley BGR model.

the crossover composition.^{8,9} We take the data of Ref. 8 and apply our self-consistent model including a line-shape fit to one of the spectra published in this reference. The population in the side minima is found to be comparable to the one in the Γ minimum. Accordingly, the density of holes is about twice as high as the Γ -point electron density. We calculate the renormalization of the fundamental gap taking into account the correct density distribution. The result is depicted in Fig. 8, where we use the density in the Γ minimum for the normalization to r_s to enable a direct comparison to Capizzi's data. The carrier temperature is chosen to increase slightly with carrier density, as is expected for an EHP. The temperature $T_e = 50$ K for the data point at $r_s = 0.83$, which is taken from our fit to the spectrum in Fig. 4 of Ref. 8, is equal to the temperature given by Capizzi *et al.* The BGR calculation has to be performed for each temperature separately. The agreement of these calculations with the experimental points is excellent. We want to point out again that the self-consistent model has no adjustable parameters. Only the input values for n and T are chosen such to fit the luminescence spectra.

This example demonstrates the effect of sidevalley populations on the narrowing of the fundamental gap. Using our multivalley model we were able to solve the question of the enhancement of the BGR in $\text{Al}_x\text{Ga}_{1-x}\text{As}$. The same behavior of the direct-band-gap renormalization is found in $\text{GaAs}_x\text{P}_{1-x}$ just below the crossover composition. Fieseler, Schwabe, and Staehli⁴⁶ treated the BGR in this multivalley system in a full RPA theory. The strong BGR of the direct gap could again be explained by the large population in the side valley. Good agreement between experiment and theory was achieved, but with the condition that the relative separation of the Γ and X minima in the unexcited sample was treated as a fit parameter. A recent application of the same model to direct-band-gap $\text{Al}_{0.30}\text{Ga}_{0.70}\text{As}$ at 2 K shows similar trends of the BGR as found in our studies.⁴⁷ Again, an adjustment of the separation between Γ and now L minima was necessary to achieve agreement between experiment and theory. Another interesting candidate for a test of the multiple-valley model would be GaSe, where a simultaneous presence of the direct and indirect EHP's was reported.⁴⁸ Corresponding calculations, however, have not been performed yet.

The effects of sidevalley population get stronger in the case of high carrier temperatures. Here, the high temperature leads to a significant population of the side valleys even for x values much smaller than x_c . The case of highly excited $\text{Al}_{0.33}\text{Ga}_{0.77}\text{As}$ at room temperature is depicted in Fig. 9. The BGR is up to 50% higher than expected for the case when only the population of the central valley is considered (see the solid line in Fig. 9). Our multivalley expansion of the universal formula again gives good agreement with the experimental points using a carrier temperature of 350 K as extracted from line-shape fits.

The applicability of our model to room temperature is not clear *a priori* but it appears to be justified in the high-density limit from the following arguments. Modifications of the many-particle interactions at high

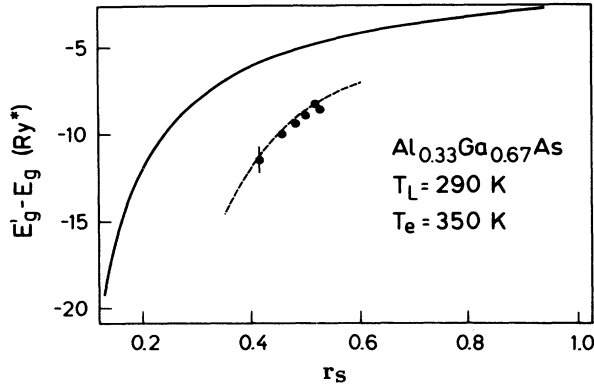


FIG. 9. Renormalization of the direct gap in $\text{Al}_{0.33}\text{Ga}_{0.67}\text{As}$ at room temperature. The carrier temperature T_e is taken from fits to the experimental spectra. The dashed line is calculated from the self-consistent multivalley model.

temperatures result only in minor deviations from the VK formula. The theory applicable to finite temperatures derived in Refs. 2 and 49 is nearly identical to the VK formula with deviations less than 2% for a large density range between 5×10^{17} and $2 \times 10^{19} \text{ cm}^{-3}$ (i.e., r_s equals 0.7 and 0.2). The temperature-induced changes of E_c and E_x actually cancel at lower carrier densities to result in small deviations between E_{xc} (300 K) and E_{xc} (0 K). In the high-density limit the energies E_c and E_x approach individually their low-temperature behaviors. A comparison to the model of Ref. 7, which uses a couple of simplifying approximations, leads to somewhat larger discrepancies. The deviations from the VK formula are, however, even here only of the order of 1 Ry^* in the density regime under consideration and in any case by a factor of 4–5 smaller than the effects due to the side-valley population. The temperature dependence is thus neglected in our model system, which is a posteriori justified by the excellent agreement with the experimental data (Fig. 9).

All these examples show that the BGR in a high-density EHP generated in a semiconductor with multiple unequivalent valleys is well described by a rather simple multiple-valley model. This model does not require lengthy many-particle calculations and is easily applicable to various scenarios in highly excited semiconductors. We will give in Sec. IV a series of examples of how the differential renormalization of the various gaps influences the optical properties in $\text{Al}_x\text{Ga}_{1-x}\text{As}$ close to the crossover composition.

IV. DIFFERENTIAL GAP RENORMALIZATION IN $\text{Al}_x\text{Ga}_{1-x}\text{As}$ CLOSE TO THE CROSSOVER COMPOSITION

A. Laser-induced direct-to-indirect transition

The first example will be the differential renormalization of the direct and indirect gaps in $\text{Al}_{0.42}\text{Ga}_{0.58}\text{As}$. This material is a direct-band-gap semiconductor at low optical excitation but an indirect-band-gap one at high-

excitation conditions.

The AlAs content of this sample was determined from high-resolution x-ray diffraction to be 0.423. The energy of the free excitons agree within few meV with the values expected from Ref. 25. We use low-excitation photoluminescence excitation (PLE) spectroscopy to determine the direct and indirect absorption edges. Only the direct absorption edge is observed in this sample without any additional step due to the indirect gap [see Fig. 10(a)]. This is in contrast to what is found in indirect samples like $\text{Al}_{0.44}\text{Ga}_{0.56}\text{As}$. Here, two steps related to the indirect and direct gaps are detected [see Fig. 10(b)]. The indirect step is easily identified from the position of the zero-phonon line related to the free X -point exciton $(\text{FE})_X$, which exactly coincides with the indirect absorption edge. The broader line at lower energies is due to impurity-bound excitons. It is interesting to note that a similar luminescence feature is found in the $\text{Al}_{0.42}\text{Ga}_{0.58}\text{As}$ sample in the time-integrated spectrum at low excitation [Fig. 10(a)]. This demonstrates that the direct and indirect gaps have to be very close in energy. We actually observe even the direct free exciton $(\text{FE})_\Gamma$ as an additional line in time-resolved luminescence at short times after the excitation. This exciton is found 2 meV above the $(\text{FE})_X$ and persists at elevated temperature above 30 K. The attribution of this additional line to the $(\text{FE})_\Gamma$ can be concluded from a detailed analysis of the dynamics, temperature, and pressure dependence of this line. More details of these studies will be given in a sub-

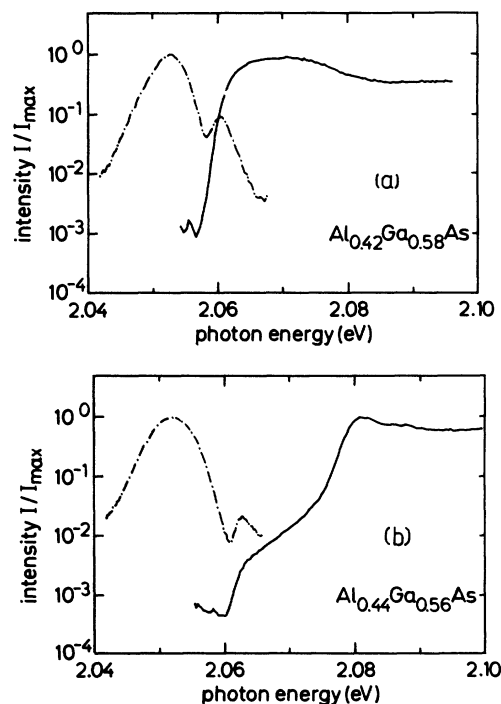


FIG. 10. Photoluminescence excitation spectra (solid lines) and low-excitation time-integrated luminescence (dashed-dotted lines) in samples close to (a) and well above (b) the crossover composition.

sequent paper.⁴¹ The simultaneous presence of $(FE)_X$ and $(FE)_\Gamma$ is a direct result of the interesting minima ordering in this sample. The binding energy of the excitons is different by almost a factor of 2, namely, 6.8 meV for the $(FE)_\Gamma$ and 11.4 meV for the $(FE)_X$. Extrapolation from the position of the exciton lines places the direct gap at 2.068 eV and the indirect slightly higher at 2.071 eV. The sample is therefore still a direct-band-gap semiconductor in the picture of the single-particle approximation. Many-particle phenomena (here the indirect excitons), however, dominate the time-integrated luminescence.

The direct exciton is actually only seen as a narrow line when this excitonic resonance is not degenerate with the indirect-exciton continuum states. Measurements in samples which are clearly indirect due to composition or hydrostatic pressure show the presence of the direct transitions only in a lifetime-broadened short emission during the picosecond excitation pulse. The exciton is very rapidly dissociated due to the fast intervalley scattering of the electron into the X or L minima.

This situation applies also to the case of high excitation in the $Al_{0.42}Ga_{0.58}As$ sample. Emission from the central valley (now band-to-band recombination) is only seen as a short luminescence during the excitation process (Fig. 11). The sample turns to an indirect-band-gap semiconductor during the excitation process. The indirect nature of the fundamental gap after the excitation pulse is evident from the luminescence signal (see the solid line in Fig. 11). The lifetime of this luminescence band is in the order of 1 ns and thus about a factor of 10 larger than the lifetime of the EHP in comparable direct-band-gap samples. The luminescence can be attributed to result from the EHP or a liquid phase whose electrons reside in the X minima depending on the excitation conditions. The properties of these plasma and liquid phases are discussed in detail in Ref. 14. The renormalized gap in the high-excitation case is determined from the low-energy tail of the luminescence to be about 40 meV below the gap in the unexcited sample in agreement with the prediction from our BGR model.

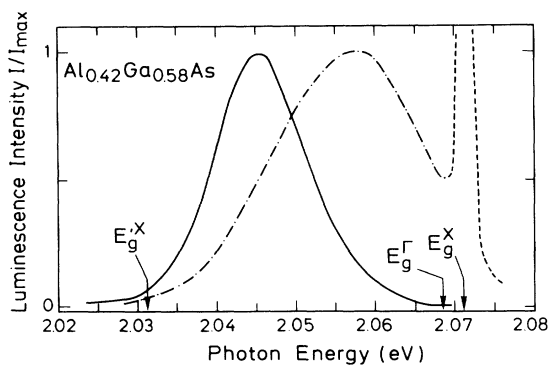


FIG. 11. Direct emission (dashed-dotted line) during the excitation process (scattered light from the laser is shown as the truncated dashed line) and indirect emission after a delay time of 200 ps (solid line) in $Al_{0.42}Ga_{0.58}As$ at $T_L = 5$ K. The arrows mark the positions of the renormalized and unrenormalized gaps.

For further studies of the differential gap renormalization, we increased the lattice temperature in the $Al_{0.42}Ga_{0.58}As$ sample to 30 K. This procedure has the consequence that the electron-hole system does not condense into a dense liquid phase. We are thus able to vary systematically the electron-hole pair density. There is further some population in the Γ minimum (about 10^{15} cm^{-3}), which gives a significant contribution to the luminescence signal even at long delay times after the excitation (see high-energy peak or shoulder in spectra of Fig. 12). The relatively strong intensity of the direct emission stems from its much higher transition probability compared to the indirect recombination (this difference in transition strength of the order of 100 is also evident from the PLE spectra in Fig. 10). The population of the X minima and thus its energy shift is, of course, a function of the excitation level, while the density in the central valley does not change significantly as a result of the differential BGR. It follows a strong decrease in the indirect emission, while the intensity of the direct luminescence signal is nearly constant when the excitation level is lowered (Fig. 12).

We again perform line-shape fits to the emission spectra in order to determine the carrier densities and the renormalized gaps (Fig. 13). The indirect emission is, as usual, treated with relaxed momentum conservation while conservation of momentum is assumed for the direct emission. The energy of the renormalized direct minimum and its population are not adjustable parameters in these fits, but calculated self-consistently. Fit parameters are the energy of the indirect gap, the common carrier temperature, and the overall density. The resulting fits to the spectra are not perfect, because we again do not include any broadening mechanism, but they are good enough to extract the relative positions of the gaps. The experimentally determined renormalized gaps are shown in Fig. 14 as a function of the overall carrier density. The figure depicts further a self-consistent calculation of the direct and indirect gaps starting from the unrenor-

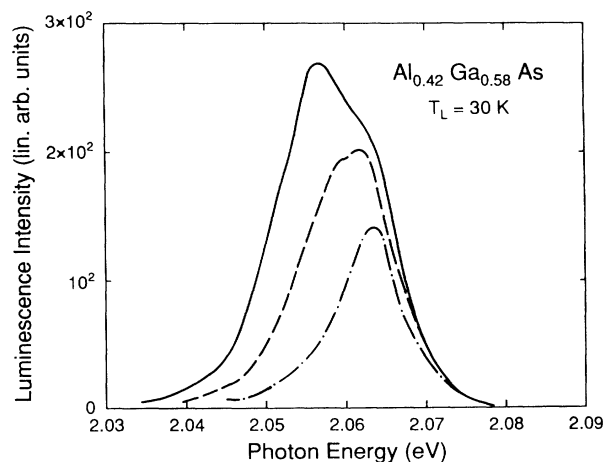


FIG. 12. Luminescence signal at long delay times ($t = 1.3$ ns) at elevated lattice temperature for different excitation levels (solid line, $F = 170 \mu\text{J}/\text{cm}^2$; dashed line, $F = 60 \mu\text{J}/\text{cm}^2$; dashed-dotted line, $F = 26 \mu\text{J}/\text{cm}^2$).

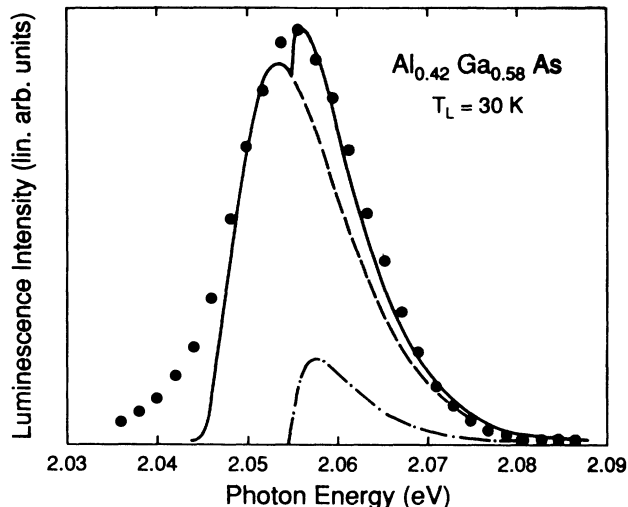


FIG. 13. Fit (solid line) to a luminescence spectrum (dots) in $\text{Al}_{0.42}\text{Ga}_{0.58}\text{As}$ including indirect (dashed line) and direct (dashed-dotted line) emission.

malized gap energies as determined from the excitonic luminescence. There is good agreement between the calculation and the experimental points. Both experiment and model demonstrate the transition from a direct-band-gap semiconductor at low excitation to an indirect-band-gap material at high carrier densities and the differential renormalization of the gaps. The excitation-induced direct-to-indirect crossover occurs at a density of about 10^{16} cm^{-3} , i.e., close to the Mott density. The nature of the fundamental gap in this semiconductor is thus determined by the excitation level.

A direct consequence of the renormalization-induced direct-to-indirect transition is a shift of the composition

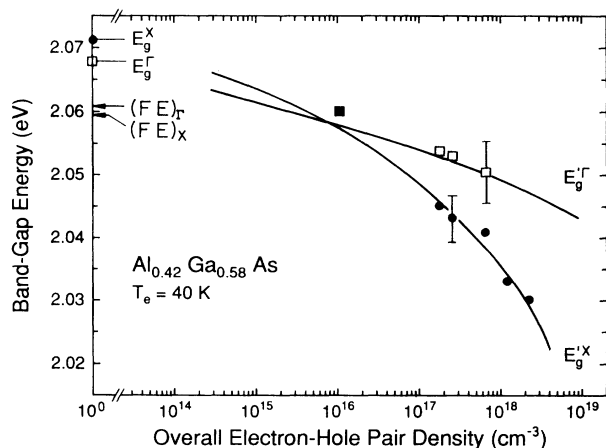


FIG. 14. Direct-to-indirect changeover as a function of carrier density. The data points for the direct (squares) and indirect (dots) gaps are extracted from line-shape fits to experimental spectra (see Figs. 12 and 13). The data points at low density are taken from excitonic luminescence spectra. The solid lines are calculated with the multivalley model for the BGR starting at the position of the unrenormalized gaps.

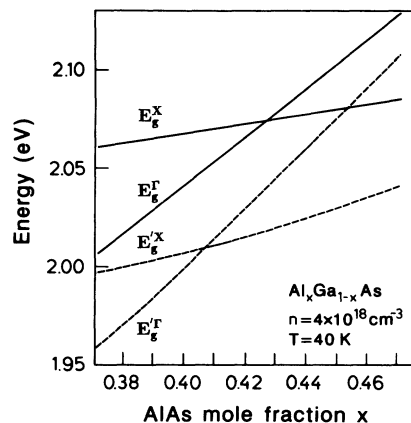


FIG. 15. Direct-to-indirect crossover in unexcited (solid lines) and highly excited (dashed lines) $\text{Al}_x\text{Ga}_{1-x}\text{As}$. The crossover shifts as a function of density from 0.426 to here 0.408.

of the crossover x_c to slightly lower x values in the case of a highly excited material. This situation is demonstrated in Fig. 15, where we show calculations with our multivalley model for a fixed carrier density. The actual ordering and position of the individual gaps is determined by the relative distribution of the population among the minima. The crossover composition is 0.408 for the chosen parameters in accordance with our experimental observations. The same effect is also found in samples close to the crossover under hydrostatic pressure. The crossover pressure is reduced in an analogous way in the case of high excitation.¹⁴ Differential band-gap renormalization and a reduced crossover pressure at high densities is also found close to the type-I to type-II transition in short-period superlattices.⁵⁰

A further example of a transition from a direct to an indirect fundamental gap is reflected in the behavior of stimulated emission in $\text{Al}_x\text{Ga}_{1-x}\text{As}$ close to the cross-

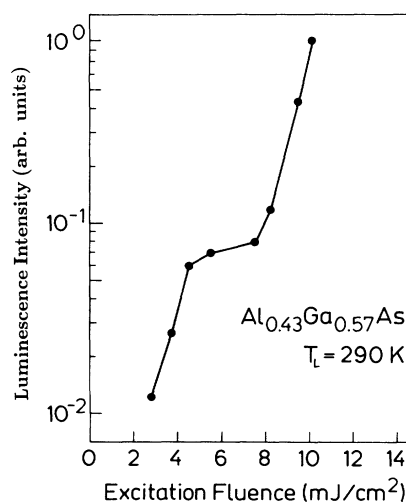


FIG. 16. Intensity of stimulated emission as a function of excitation level $\text{Al}_{0.43}\text{Ga}_{0.57}\text{As}$ at room temperature. The solid line is a guide for the eye.

over composition. Stimulated emission is possible in this semiconductor alloy for recombination of the electrons in all three valleys of the conduction band. Direct stimulated emission dominates for x values below x_c , while indirect stimulated transitions of X -point electrons to the valence band are observed for $x > x_c$.^{30,31,51,52} The latter process is a zero-phonon recombination induced by the alloy disorder, the transition probability of which is well described by second-order perturbation theory.^{31,53} The electron recombines here via a virtual intermediate state in the Γ minimum. The energy separation between X and Γ minima thus determines via an energy denominator the efficiency of this indirect stimulated emission. The efficiency is, of course, highest when central and side valleys are nearly degenerate.

From the temperature dependence of the threshold fluence for optically pumped stimulated emission we were able to demonstrate that $\text{Al}_{0.43}\text{Ga}_{0.57}\text{As}$ changes from an indirect to a direct gap semiconductor as a function of lattice temperature.⁵⁴ The crossover occurs at about 80 K. The stimulated emission in this sample is thus direct at room temperature, but the side valleys at the X and L points are still close by in energy. With increasing carrier density it is thus possible to switch the stimulated emission for this composition from direct to indirect. The intensity of the stimulated luminescence as a function of excitation fluence (Fig. 16) demonstrates this behavior. The intensity rises steeply with excitation level but reaches a saturation level around 8 mJ/cm^2 . With increasing pump fluence it is then possible to rise the carrier density in the sample. The relatively large density in the high-mass side valleys finally leads to a crossing of the X minima below the Γ minimum. This can be shown by a calculation of the renormalized band gaps as a function of carrier density (see Fig. 17). The direct-to-indirect transition is reflected in the stimulated emission by a sudden steep rise in the emission intensity at 11 mJ/cm^2 when the indirect channel gets dominant. The crossing of L and Γ minima results in a strong fluctuation of the emission level at higher pump fluences (see Ref. 55 for more details). A similar behavior induced by minima crossing, but without a change in the nature of the fundamental gap, will be discussed in the following section.

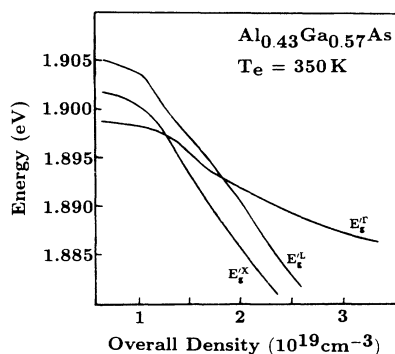


FIG. 17. Band-gap energies and minima crossing as a function of the overall carrier density in $\text{Al}_{0.43}\text{Ga}_{0.57}\text{As}$ calculated with the multivalley model.

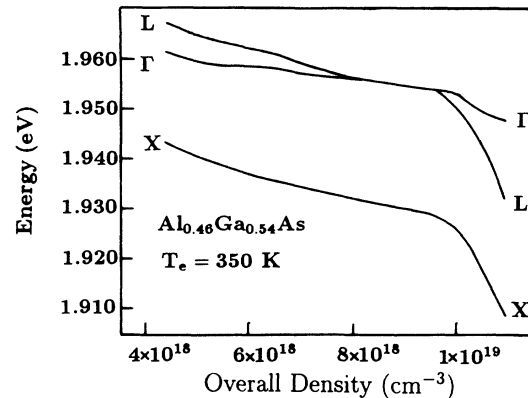


FIG. 18. Band-gap energies and minima crossing as a function of the overall carrier density in $\text{Al}_{0.46}\text{Ga}_{0.54}\text{As}$ calculated with the multivalley model.

B. Influence of L - Γ crossing on indirect stimulated emission

The stimulated transition in $\text{Al}_{0.46}\text{Ga}_{0.54}\text{As}$ is indirect at all pump levels at room temperature. The origin of the involved electrons, however, can change from the X to

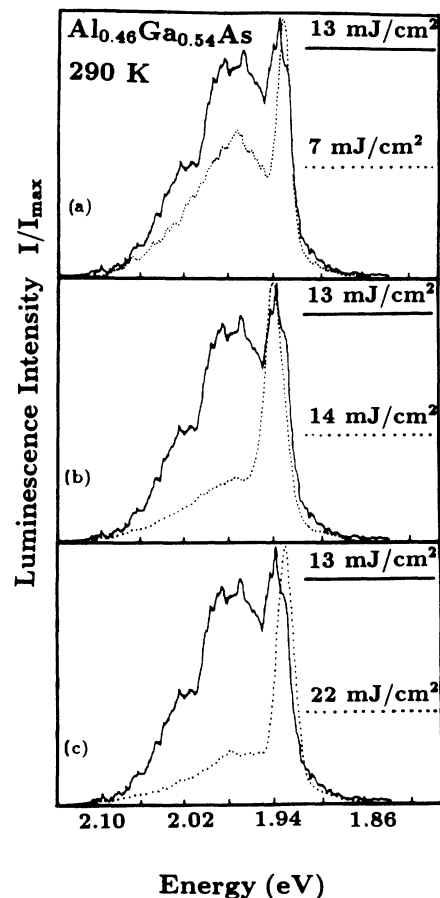


FIG. 19. Stimulated and spontaneous emission in $\text{Al}_{0.46}\text{Ga}_{0.54}\text{As}$ at various excitation levels.

the L minima. A calculation of the renormalized band gaps shows that a crossing of the L and Γ minima is expected in the density range around $1 \times 10^{19} \text{ cm}^{-3}$ as a consequence of the differential renormalization (Fig. 18). The L minima are thus close to energetical degeneracy with the central valley. This results in a very large transition probability due to the small energy denominator in the matrix element. The rather high population of the L valleys at room temperature then dominates the stimulated emission process in this density range.

This change in the transition channel is proven by the behavior of the stimulated emission. The emission above the threshold is positioned at the low-energy tail of the spontaneous luminescence, i.e., at the indirect X gap [see Fig. 19(a), $F=7 \text{ mJ/cm}^2$]. The efficiency of the stimulated process drops dramatically when the pump fluence is enlarged to 13 mJ/cm^2 . Simultaneously, additional emission bands are observed on the high-energy side of both, the stimulated and the spontaneous emission. The position of the stimulated emission line jumps to higher photon energies by 25 meV and the intensity rises significantly with further increase of the pump fluence by only one 1 mJ/cm^2 [Fig. 19(b)]. This shift in emission energy corresponds exactly to the energy separation between the L and the X minima at the crossing of L and Γ (see Fig. 18). The behavior of the stimulated emission is thus identified to result from the change in the dominant recombination channel from transitions involving the X minima to ones involving the L minima. The dominance of the emission from the L minima is a direct consequence of the close to resonance condition of these conduction-band minima, while the X minima are much further separated from the intermediate states. With further increase of the excitation density the dominant stimulated emission changes back to the X minima, because the much larger population inversion eventually compensates for the smaller transition probability. At 22 mJ/cm^2 the emission is again related to the lowest indirect gap and the emission at higher photon energies has ceased [Fig. 19(c)].

V. SUMMARY

The band-gap renormalization in semiconductors with multiple inequivalent valleys can be described by a multivalley expansion of the universal formula of Vashishta and Kalia. The main modification in this expansion is the explicit treatment of the electron-exchange interaction in each individual minimum. This model is able to describe the shift of essentially unoccupied conduction-band minima at higher energies, as well as the renormalization of partially occupied minima in a self-consistent treatment. The model calculations are in excellent agreement with experimental data in both direct-band-gap and indirect-band-gap $\text{Al}_x\text{Ga}_{1-x}\text{As}$ for the fundamental and higher-energy band gaps. The differential renormalization of minima with different effective masses and thus populations leads to laser-induced crossings of various minima such as a changeover from a direct to an indirect semiconductor in $\text{Al}_x\text{Ga}_{1-x}\text{As}$ close to the crossover point. Minima crossings further influence the dominant recombination channel, the efficiency, and the emission wavelength of indirect stimulated emission.

ACKNOWLEDGMENTS

One of us (H.K.) gratefully acknowledges the very fruitful collaboration in the early stages of this work with K. Bohnert, A. L. Smirl, T. F. Boggess, and D. P. Norwood at the Center for Applied Quantum Electronics in Denton, Texas. We are further most grateful for very useful support from W. W. Rühle and K. Reimann at the Max-Planck-Institut für Festkörperforschung in Stuttgart (FRG), and helpful discussions with R. Zimmermann. The excellent samples used in our studies were grown by F. Bantien, E. Bauser, Y.-C. Lu, K. Köhler, P. Ganser, and I. J. D'Haenens. We finally acknowledge the expert technical assistance by K. Rother and H. Klann.

*Present address: Fachbereich Physik der Universität, Erwin-Schrödinger-Strasse, D-6750 Kaiserslautern, Federal Republic of Germany.

¹H. Haug and S. Schmitt-Rink, *Prog. Quant. Electron.* **9**, 3 (1984).

²R. Zimmermann, *Many-Particle Theory of Highly Excited Semiconductors* (Teubner, Leipzig, 1988).

³*Optical Nonlinearities and Instabilities in Semiconductors*, edited by H. Haug (Academic, New York, 1988).

⁴T. M. Rice, in *Solid State Physics*, edited by H. Ehrenreich, F. Seitz, and D. Turnbull (Academic, New York, 1977), Vol. 32, p. 1.

⁵P. Vashishta and R. K. Kalia, *Phys. Rev. B* **25**, 6492 (1982).

⁶P. Vashishta, R. K. Kalia, and K. S. Singwi, in *Electron-Hole Droplets in Semiconductors*, edited by C. D. Jeffries and L. V. Keldysh (North-Holland, Amsterdam, 1983), p. 1.

⁷H. Haug and S. W. Koch, *Phys. Rev. A* **39**, 1887 (1989).

⁸M. Capizzi, S. Modesti, A. Frova, J. L. Staehli, M. Guzzi, and R. A. Logan, *Phys. Rev. B* **29**, 2028 (1984).

⁹K. Bohnert, H. Kalt, A. L. Smirl, D. P. Norwood, T. F. Boggess, and I. J. D'Haenens, *Phys. Rev. Lett.* **60**, 37 (1988).

¹⁰H. Kalt, K. Bohnert, A. L. Smirl, and T. F. Boggess, in *Proceedings of the 19th International Conference on the Physics of Semiconductors*, edited by W. Zawadzki (Polish Academy of Science, Warsaw, 1988), p. 1377.

¹¹M. Rinker, H. Kalt, K. Reimann, Y.-C. Lu, and E. Bauser, *Phys. Rev. B* **42**, 7274 (1990); H. Kalt, K. Reimann, M. Rinker, W. W. Rühle, and E. Bauser, in *Proceedings of the 20th International Conference on the Physics of Semiconductors*, edited by E. M. Anastassakis and J. D. Joannopoulos (World Scientific, Singapore, 1990), p. 2498.

¹²G. W. Fehrenbach, W. Schäfer, J. Treusch, and R. G. Ulbrich, *Phys. Rev. Lett.* **49**, 1281 (1982).

¹³J. C. Hensel, T. G. Phillips, and G. A. Thomas, in *Solid State Physics*, Ref. 4, p. 88.

¹⁴H. Kalt, K. Reimann, W. W. Rühle, M. Rinker, and E. Bauser, *Phys. Rev. B* **42**, 7058 (1990).

¹⁵A. Forchel, H. Schweitzer, and G. Mahler, *Phys. Rev. Lett.*

- 51, 501 (1983).
- ¹⁶M. Rösler and R. Zimmermann, *Phys. Status Solidi B* **83**, 85 (1977).
- ¹⁷R. Zimmermann, E. H. Böttcher, N. Kirstaedter, and D. Bimberg, *Superlatt. Microstruct.* **7**, 433 (1990).
- ¹⁸K. H. Schlaad, Ch. Weber, J. Cunningham, C. V. Hoof, G. Borghs, G. Weimann, W. Schlapp, H. Nickel, and C. Klingshirn, *Phys. Rev. B* **43**, 4268 (1991).
- ¹⁹V. D. Kulakovskii, E. Lach, A. Forchell, and D. Grützmacher, *Phys. Rev. B* **40**, 8087 (1989).
- ²⁰G. Bongiovanni, J. L. Staehli, A. Bosacchi, and S. Franchi, *Superlatt. Microstruct.* **9**, 479 (1991).
- ²¹W. H. Knox, C. Hirlimann, D. A. B. Miller, J. Shah, D. S. Chemla, and C. V. Shank, *Phys. Rev. Lett.* **56**, 1191 (1986).
- ²²W. F. Brinkmann and T. M. Rice, *Phys. Rev. B* **7**, 1508 (1973).
- ²³H. C. Casey and M. B. Panish, *Heterostructure Lasers* (Academic, New York, 1978), Pt. A.
- ²⁴S. M. Sze, *Physics of Semiconductor Devices* (Wiley, New York, 1981).
- ²⁵D. J. Wolford, W. Y. Hsu, J. D. Dow, and B. G. Streetman, *J. Lumin.* **18/19**, 863 (1978).
- ²⁶H. Kroemer, *Surf. Sci.* **174**, 299 (1986).
- ²⁷H. Kalt, W. W. Rühle, K. Reimann, M. Rinker, and E. Bauser, *Phys. Rev. B* **43**, 12364 (1991).
- ²⁸H. Kalt, W. W. Rühle, and K. Reimann, *Solid State Electron.* **32**, 1819 (1989).
- ²⁹H. Kalt, K. Bohnert, D. P. Norwood, T. F. Boggess, A. L. Smirl, and I. J. D'Haenens, *J. Appl. Phys.* **62**, 4187 (1987).
- ³⁰H. Kalt, A. L. Smirl, and T. F. Boggess, *J. Appl. Phys.* **65**, 294 (1989).
- ³¹M. Rinker, H. Kalt, and K. Köhler, *Appl. Phys. Lett.* **57**, 284 (1990).
- ³²C. Lasher and F. Stern, *Phys. Rev.* **133**, A553 (1964).
- ³³J. S. Blakemore, *J. Appl. Phys.* **53**, R123 (1982).
- ³⁴V. C. Aguilera-Navarro, G. A. Estevez, and A. Kostecki, *J. Appl. Phys.* **63**, 2848 (1988).
- ³⁵X. Aymerich-Humet, F. Serra-Mestres, and J. Millan, *Solid State Electron.* **24**, 981 (1981).
- ³⁶R. W. Martin and H. L. Störmer, *Solid State Commun.* **22**, 523 (1977).
- ³⁷E. Hess, I. Topol, K. R. Schulze, H. Neumann, and K. Unger, *Phys. Status Solidi B* **55**, 187 (1973).
- ³⁸B. Reinländer, H. Neumann, P. Fischer, and G. Kühn, *Phys. Status Solidi B* **48**, K167 (1972).
- ³⁹S. Adachi, *J. Appl. Phys.* **58**, R1 (1985).
- ⁴⁰P. Lawaetz, *Phys. Rev. B* **4**, 3460 (1971).
- ⁴¹H. Kalt (unpublished).
- ⁴²W. W. Rühle, K. Leo, and E. Bauser, *Phys. Rev. B* **40**, 1756 (1989).
- ⁴³H. Haug and D. B. Tran Thoai, *Phys. Status Solidi B* **98**, 581 (1980).
- ⁴⁴A. Selloni, S. Modesti, and M. Capizzi, *Phys. Rev. B* **30**, 821 (1984).
- ⁴⁵H. Schweitzer, A. Forchel, A. Hangleiter, S. Schmitt-Rink, J. P. Löwenau, and H. Haug, *Phys. Rev. Lett.* **51**, 698 (1983).
- ⁴⁶H. Fieseler, R. Schwabe, and J. L. Staehli, *Phys. Status Solidi B* **159**, 411 (1990).
- ⁴⁷H. Fieseler, R. Schwabe, K. Unger, and J. L. Staehli, in *Proceedings of the 20th International Conference on the Physics of Semiconductors*, edited by E. M. Anastassakis and J. D. Joannopoulos (World Scientific, Singapore, 1990), p. 1093.
- ⁴⁸R. Cingolani, M. Ferrara, and M. Lugara, *Phys. Rev. B* **36**, 9589 (1989).
- ⁴⁹M. Rösler, R. Zimmermann, and W. Richert, *Phys. Status Solidi B* **121**, 609 (1984).
- ⁵⁰J. Nunnenkamp, K. Reimann, J. Kuhl, and K. Ploog (unpublished).
- ⁵¹E. Cohen, M. D. Sturge, M. A. Olmstead, and R. A. Logan, *Phys. Rev. B* **22**, 771 (1980).
- ⁵²R. Sarfaty, Arza Ron, E. Cohen, and R. A. Logan, *J. Appl. Phys.* **59**, 780 (1986).
- ⁵³A. N. Pikhtin, *Fiz. Tekh. Poluprov.* **11**, 425 (1977) [*Sov. Phys. Semicond.* **11**, 245 (1977)].
- ⁵⁴M. Rinker, H. Kalt, Y.-C. Lu, E. Bauser, P. Ganser, and K. Köhler, *Appl. Phys. Lett.* **59**, 1102 (1991).
- ⁵⁵M. Rinker, H. Kalt, Y.-C. Lu, E. Bauser, K. Köhler, and P. Ganser, *Appl. Phys. A* **53**, 198 (1991).